Mobility of a class of perforated polyhedra

Patrick W. Fowler*

Department of Chemistry
University of Sheffield
Sheffield S3 7HF, UK
P.W.Fowler@sheffield.ac.uk

Simon D. Guest

Department of Engineering
University of Cambridge
Trumpington Street, Cambridge CB2 1PZ, UK
sdg@eng.cam.ac.uk

Bernd Schulze[1]

Department of Mathematics and Statistics
Lancaster University
Lancaster LA1 4YF, UK
b.schulze@lancaster.ac.uk

Abstract

A class of over-braced but typically flexible body-hinge frameworks is described. They are based on polyhedra with rigid faces where an independent subset of faces has been replaced by a set of holes. The contact polyhedron C describing the bodies (vertices of C) and their connecting joints (edges of C) is derived by subdivision of the edges of an underlying cubic polyhedron. Symmetry calculations detect flexibility not revealed by counting alone. A generic symmetry-extended version of the Grübler-Kutzbach mobility counting rule accounts for the net mobilities of infinite families of this type (based on subdivisions of prisms, wedges, barrels, and some general inflations of a parent polyhedron). The prisms with all faces even and all barrels are found to generate flexible perforated polyhedra under the subdivision construction.

The investigation was inspired by a question raised by Walter Whiteley

[1]Supported by EPSRC First Grant EP/M013642/1

about a perforated polyhedron with a unique mechanism reducing octahedral to tetrahedral symmetry. It turns out that the perforated polyhedron with highest ($\mathcal{O}_h$) point-group symmetry based on subdivision of the cube is mechanically equivalent to the Hoberman Switch-Pitch toy. Both objects exhibit an exactly similar mechanism that preserves $\mathcal{T}_d$ subgroup symmetry over a finite range; this mechanism survives in two variants suggested by Bob Connelly and Barbara Heys that have the same contact graph, but lower initial maximum symmetry.

Keywords: rigidity, mobility, cubic polyhedron, symmetry

---

1. Introduction

A trend in the treatment of mobility of frameworks composed of arrays of bodies connected by hinges is of the application of symmetry, wherever possible, to the counting of net mobility $m - s$, the balance of freedoms and constraints (or equivalently of mechanisms and states of self-stress) [11, 12, 19, 5, 21, 22, 32, 28, 31]. One particular flexible framework realised as a Polydron$^{\text{TM}}$ model was described in a 2014 Fields Institute lecture by Walter Whiteley, at a meeting held to mark his 70th birthday; his observation of a symmetry-breaking mechanism of the model inspired the present investigation of an open-ended class of mobile frameworks based on the cubic polyhedra.

The basic object that sparked this investigation is W. Two further variants, R and B, emerged in discussions with Bob Connelly and Barbara Heys. In W six disjoint square faces of an octahedrally symmetric Archimedean polyhedron, the (small) rhombicuboctahedron [7], have been replaced by holes. B is also derived from this polyhedron. R is derived from the pseudo-rhombicuboctahedron discovered by Miller, as described in [29]. All three objects are illustrated in Figure 1. All exhibit a symmetry-breaking finite mechanism. Application of the established techniques for symmetry extension of mobility rules [19] leads to an account of net mobility in all three structures. Interestingly, the explanation for the finite mechanism in W, which takes the structure from octahedral $\mathcal{O}_h$ to tetrahedral $\mathcal{T}_d$ symmetry, turns out to be identical with the symmetry account of the mechanism of the famous Hoberman Switch-Pitch toy [23, 4]

The motivation for our symmetry treatment of an infinite class of structures is the initially surprising flexibility of some heavily over-constrained

(a)

(b)

(c)

Figure 1: Physical models of W, R and B, constructed from Magnetic Polydron^{TM} components. Rows (a), (b) and (c) correspond to W, R and B, respectively. Each row shows points on the path of the characteristic mechanism: initial high-symmetry configuration; the distortion mechanism, showing the halving of the symmetry group; the fully collapsed configuration after the pathway has passed through the multifurcation.

objects. W is an object with maximum octahedral rotational and reflectional symmetry belonging to the point group $\mathcal{O}_h$, which has 48 symmetry operations. Although over-braced by six states of self-stress according to simple counting, this framework has a mechanism that preserves the 24 symmetries of the tetrahedral $\mathcal{T}_d$ point group along a finite path that proceeds down from the high-symmetry point until a special geometry is reached where multifurcation into lower symmetries takes place. The multi-branched pathway for further distortion starts at the point where each of four square faces becomes co-planar with its neighbours and can individually move radially in or out. Variants R ($\mathcal{C}_{4v}$) and B ($\mathcal{D}_{4h}$) show similar mechanisms that lead to halving of the symmetry group, with branching, and the possibility of further symmetry loss, at the co-planarity point or points. Figure 1 shows snapshots along the path of the mechanism in W, R and B. In the following, we use the symmetry-extended mobility criterion to place the flexes of W, R and B in the context of infinite families of perforated polyhedra.

While we restrict attention to symmetric structures and their symmetry-induced mobility in this paper, we note that the mobility analysis of *generic* perforated polyhedral structures (without symmetry), under the term 'block-and-hole' polyhedra, is currently also an active area of research. In particular, it was shown in [10] that under certain conditions, a generic embedding of a simplicial spherical polyhedron (which is rigid by Cauchy's rigidity theorem) remains rigid if a triangulated disc is cut out and new constraints are added into an essentially disjoint disc to create a rigid sub-structure (or rigid block). This result was very recently extended to structures with one rigid block and an arbitrary number of holes [6]. Moreover, it was shown in [9, 6] that swapping the rigid blocks for holes and vice versa does not alter the rigidity properties of these perforated structures. The approach used here suggests that investigation of symmetry aspects of these general results for block-and-hole polyhedra and block-hole exchange would be a natural next step. This extension is currently in progress.

2. Symmetry-extended mobility criteria

The classic [24] counting criterion for mobility (relative freedoms) $m - s$ of a mechanical linkage composed of n bodies connected by g joints is

$$m - s = 6(n-1) - 6g + \sum_{i=1}^{g} f_i, \tag{1}$$

where the mobility is defined by the difference between the number of mechanisms (m) and states of self-stress (s), and each joint i permits f_i relative freedoms.

As discussed elsewhere [19], this counting criterion can be derived formally by supposing one body to be fixed, then allowing for the six relative freedoms of each of the other $(n-1)$ bodies, then counting constraints by considering each joint to remove six freedoms but to restore f_i of them. Effectively, we are supposing the system to be at first rigidly glued but then to be freed up at each joint by the appropriate number of allowed freedoms.

The symmetry extension of (1) for a linkage in a starting position with point group $\mathcal{G}$ is expressed in terms of representations of the group, Γ, and properties of the contact polyhedron C. It is [19]

$$\Gamma(m) - \Gamma(s) = (\Gamma(v, C) - \Gamma_{\parallel}(e, C) - \Gamma_0) \times (\Gamma_T + \Gamma_R) + \Gamma_{\text{freedoms}}, \qquad (2)$$

where $\Gamma(m)$ and $\Gamma(s)$ are the representations of the mechanisms and states of self-stress. In this equation, $\Gamma(v, C)$ is the permutation representation of the vertices of C. (A permutation representation of a set has character $\chi(S)$ for operation S equal to the number of objects in the set that are left in place by the operation S.) $\Gamma_{\parallel}(e, C)$ is the representation of a set of vectors along the edges of C and has characters that depend on the number of edges unshifted under a given operation and on the effect of the operation on the directions of vectors along those edges. Γ_0 is the totally symmetric representation ($\Gamma(S) = 1$ for all S); Γ_T and Γ_R are respectively the representations of rigid-body translations and rotations. Lastly, the term Γ_{freedoms} is the representation of the total set of freedoms notionally restored by the unfreezing of joints in the procedure described above. We will also find useful the antisymmetric representation, Γ_ϵ, which has characters $\chi(S) = 1$ for proper operations and $\chi(S) = -1$ for improper operations.

The notion of the contact polyhedron C encapsulates the relationships between bodies and joints: each rigid element is associated with a vertex of C, and each joint is associated with an edge. C is embedded in space, and $\mathcal{G}$ is the point group of the embedded structure. The vertices of C are embedded in the appropriate $2D$ or $3D$ space, in a geometry that is consistent with the point group symmetry of the array of bodies and joints. Thus, C may have undetermined lengths and angles, where the symmetry allows. The term 'contact polyhedron' can be a misnomer, as C is not always three-connected and may sometimes have a non-planar graph, but it seems to be the term that is used for this object: 'embedded contact graph' would be more precise.

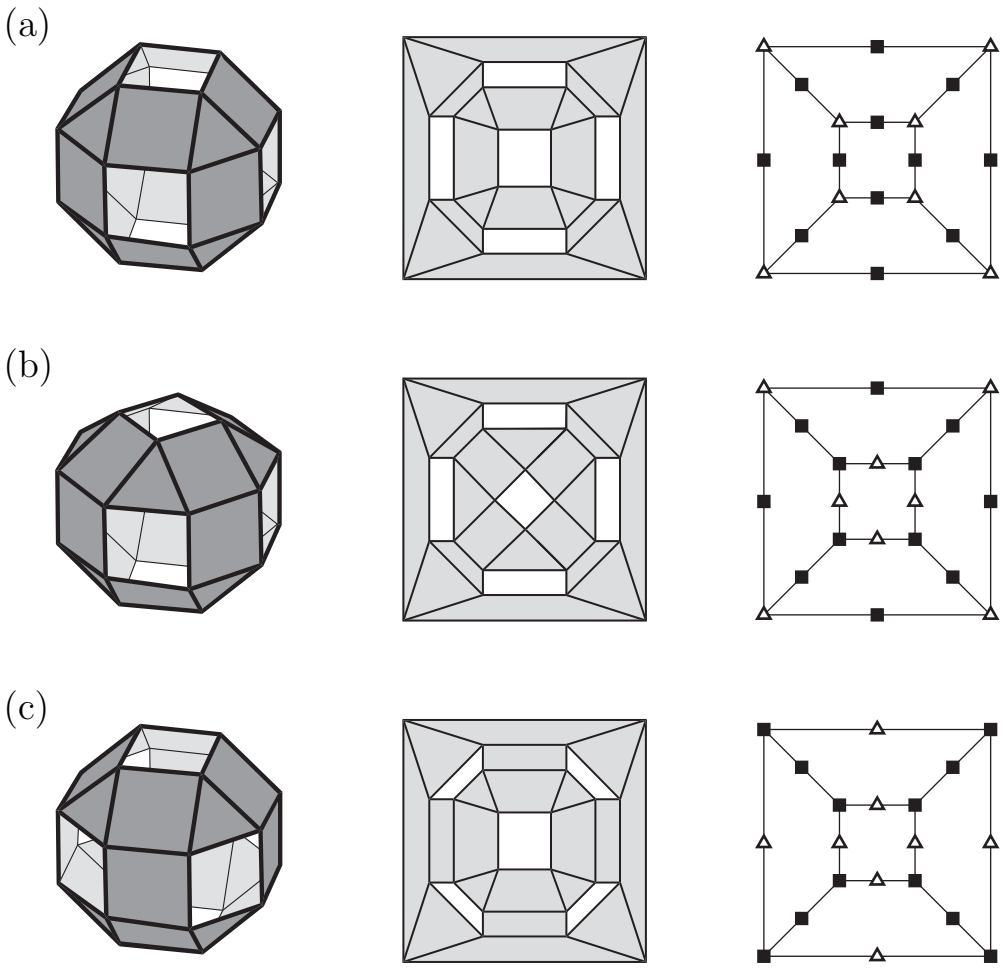

Figure 2: Three perforated polyhedral structures based on the Whiteley example, shown as three-dimensional skeletons, Schlegel diagrams, and contact graphs. (a) The Whiteley structure (W) is derived by removing six disjoint square faces that occupied the octahedral positions in the Archimedean small rhombicuboctahedron [7]. (b) Variant R is obtained by rotating the top layer of W by $\pi/4$ about a fourfold axis. (c) Variant B is obtained by rotating the middle layer instead. The three structures have related Schlegel diagrams (shown with holes unshaded) and all have the same contact graph C (that of a subdivided cube), but with different identifications between the 12 square and 8 triangular bodies and the vertices of C.

All the terms in (2) are either calculated for the particular structure $(\Gamma(v,C), \Gamma_{\parallel}(e,C), \Gamma_{\text{freedoms}})$ or are determined by the group and can be looked up in standard character tables [1, 2]. The freedoms term is determined by simple physical reasoning. In the case we envisage here, the bodies are placed at the vertices and edge-midpoints of some polyhedron P. The graph of C is then the subdivision of the graph of P (which, of course, means that C is not a polyhedron, as it is only 2-connected). The joints correspond to the edges of the subdivision, two for each original edge of P, and each is a non-torsional hinge (i.e., has a hinge line that is not collinear with the line of centres of the bodies that the hinge connects). The freedom allowed by the joint in this case is a relative rotation of the two connected bodies about the hinge line. When C lies on a spherical shell, as here, this relative rotation is fully symmetric under any operation that preserves the associated edge of C. Hence, Γ_{freedoms} in (2) can be replaced by $\Gamma(e,C)$, the permutation representation of the edges of C, to give the specific body-hinge form of the symmetry-extended mobility equation appropriate to W and to structures like it:

$$\Gamma(m) - \Gamma(s) = (\Gamma(v,C) - \Gamma_{\parallel}(e,C) - \Gamma_0) \times (\Gamma_T + \Gamma_R) + \Gamma(e,C). \quad (3)$$

Figure 2 shows the skeletons, Schlegel diagrams and contact graphs of the three objects W, R and B. Their mobility is explored in the next section. Figure 3 defines the conventions used for the settings of the symmetry groups that feature in the discussion.

3. Mobility of the Whiteley structure and variants

The equation (3) can be applied directly to the W framework and its variants R and B. In the tabular form that we have used elsewhere [11, 19], the calculation of characters for W at the high-symmetry point is
This gives the reducible representation

$$(\mathrm{W}, \mathcal{O}_h): \qquad \Gamma(m) - \Gamma(s) = A_{2u} - A_{1u} - T_{1g} - T_{2u}, \quad (4)$$

and tells us that there are at least seven states of self-stress spanning symmetries A_{2u} (one) and T_{1g} and T_{2u} (three each) and at least one mechanism of symmetry A_{1u}. The scalar count (1) gives, with $n = 20$, $g = 24$, and $f_i = 1$ for all i: $m - s = 6(20-1) - 6 \times 24 + 24 \times 1 = -6$, telling us only that the structure is over-braced, with an excess of 6 states of self-stress over mechanisms.

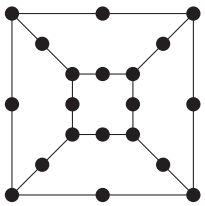

Figure 3: Generic contact graph C for structures W, R and B. The bodies occupy the vertices of the subdivided cube, and the hinges are represented by the edges. For the purpose of using symmetry to give labels to mechanisms and states of self-stress, the groups $\mathcal{O}_h$, $\mathcal{C}_{4v}$ and $\mathcal{D}_{4h}$ are chosen such that the class of σ_d reflection planes always includes the symmetry plane that runs diagonally from lower left to upper right in the Schlegel diagram of C, i.e., including six vertices of C. In all three groups, x lies along the horizontal axis of the diagram, y along the vertical axis and z is normal to the plane of the paper. In this convention the unique mechanism, which preserves the special σ_d plane for all three perforated polyhedra, has the symmetry of the xyz cubic harmonic.

$\mathcal{O}_h$	E	$8C_3$	$6C_2$	$6C_4$	$3C_4^2$	i	$6S_4$	$8S_6$	$3\sigma_h$	$6\sigma_d$
$\Gamma(v,C)$	20	2	2	0	0	0	0	0	4	6
$-\Gamma_{\parallel}(e,C)$	−24	0	0	0	0	0	0	0	0	−4
$-\Gamma_0$	−1	−1	−1	−1	−1	−1	−1	−1	−1	−1
	−5	1	1	−1	−1	−1	−1	−1	3	1
$\times(\Gamma_T+\Gamma_R)$	6	0	−2	2	−2	0	0	0	0	0
	−30	0	−2	−2	2	0	0	0	0	0
Γ_{freedoms}	24	0	0	0	0	0	0	0	0	4
	−6	0	−2	−2	2	0	0	0	0	4

Hence, counting without symmetry has shown the structure to be over-constrained, with at least six states of self-stress. Symmetry has revealed the existence of a mechanism, balanced by a total of *seven* symmetry-detected states of self-stress; the A_{2u} mechanism is one-dimensional (as it is of type A) but is symmetry-breaking in the full $\mathcal{O}_h$ point group (as it is not of type A_{1g}).

Motion along the mechanism reduces the point group symmetry to the group composed of those operations of $\mathcal{O}_h$ for which A_{2u} has character $+1$. This group is $\mathcal{T}_d$. In the lower symmetry, the mobility representation is

$$(\mathrm{W},\mathcal{T}_d): \qquad \Gamma(m)-\Gamma(s)=A_1-A_2-2T_1. \tag{5}$$

As there is no state of self-stress of A_1 symmetry to block the mechanism [25, 20, 30], the mechanism is finite. Manipulation of the physical model suggests that there is no other mechanism in the initial tetrahedral structures. In principle, the symmetry calculation gives only lower bounds on the numbers of mechanisms and states of self-stress, as there could be equisymmetric mechanisms and states of self-stress with cancelling contributions to the total $\Gamma(m) - \Gamma(s)$ and hence undetectable by symmetry. In particular, symmetry has nothing to say about the location of the multifurcation point that appears further down the A_{2u} pathway, as the additional mobility at that point depends on a specific geometry at which sets of faces become coplanar.

The mechanism has the same symmetry as the xyz cubic harmonic in both symmetry groups: A_{2u} in $\mathcal{O}_h$, A_1 in $\mathcal{T}_d$.

Mobility of the other two variant structures can be calculated in a similar way. Variant R has $\mathcal{C}_{4v}$ symmetry and could be treated by making a new table for this group, but as R and W have the same contact graph, the result follows by descent in symmetry, by simply deleting irrelevant operations from the W table. The scalar count is $m - s = -6$, as before, since scalar counting corresponds to taking the character under the identity operation. The symmetry count (in the setting of $\mathcal{C}_{4v}$ indicated in Figure 3) is

$$(\mathrm{R}, \mathcal{C}_{4v}): \qquad \Gamma(m) - \Gamma(s) = B_2 - 2A_2 - B_1 - 2E, \tag{6}$$

with the finite B_1 mechanism now leading initially to a $\mathcal{C}_{2v}$ point group in a setting where the σ_d mirror planes of the structure are preserved, and where the mobility detected by symmetry is

$$(\mathrm{R}, \mathcal{C}_{2v}): \qquad \Gamma(m) - \Gamma(s) = A_1 - 3A_2 - 2B_1 - 2B_2. \tag{7}$$

The interpretation is the same as for W, with appropriate changes to representation labels. Again, the mechanism has the symmetry of the xyz harmonic.

For the third variant, B, the calculation is similar. In maximum symmetry, B has the dihedral $\mathcal{D}_{4h}$ symmetry, which is again a subgroup of $\mathcal{O}_h$. The result for the mobility representation is

$$(\mathrm{B}, \mathcal{D}_{4h}): \qquad \Gamma(m) - \Gamma(s) = B_{1u} - A_{2g} - E_g - A_{1u} - B_{2u} - E_u, \tag{8}$$

with the symmetry-detected B_{1u} mechanism leading to structures with point group $\mathcal{D}_{2d}$ and

$$(\mathrm{B}, \mathcal{D}_{2d}): \qquad \Gamma(m) - \Gamma(s) = A_1 - 2A_2 - B_1 - 2E. \tag{9}$$

Once more, the mechanism is equisymmetric with the cubic harmonic xyz.

The mechanism is 'generic' for the three subdivisions of the graph of the cube. The full octahedral symmetry of W is in a sense an accident; the mechanism survives in the group of the more general square prism (B) and the group of the square pyramid (R) where the symmetry elements that exchange top and bottom faces of the prism are lost. We can also imagine general versions of W, R and B based on $[n]$-prisms, with groups $\mathcal{D}_{nh}$, $\mathcal{C}_{nv}$ and $\mathcal{D}_{nh}$. These will be discussed below.

Structure W is based on a decoration of the cube, but analogous structures belonging to the tetrahedral and icosahedral point groups are also easily envisaged. Experimentally, removal of an independent set of four triangular faces from the cuboctahedron (with 12 vertices, 6 square and 8 triangular faces) is found to give a rigid structure. Analysis in the $\mathcal{T}_d$ group gives the result

$$\Gamma(m) - \Gamma(s) = -A_1 - E - T_2, \tag{10}$$

corresponding exactly to the six states of self-stress implied by the scalar count of -6. Experimentation with the physical model confirms that no mechanism has been missed out in this case. An explanation of 'why' the states of self-stress representation has the particular form $A_1 + E + T_2$ follows from detailed considerations about the symmetries of cubic polyhedra (see Section 4).

Analogous reasoning for the icosahedrally symmetric small rhombicosidodecahedron [7] (which has 60 vertices, 12 pentagonal faces, each to be replaced by holes, 30 square and 20 triangular faces) gives a result that reveals a triply degenerate mechanism for the high-symmetry $\mathcal{I}_h$ structure:

$$\Gamma(m) - \Gamma(s) = T_{2u} - A_u - T_{1g} - H_u. \tag{11}$$

There are multiple distortive pathways that take the structure down five-fold, three-fold and two-fold branches of the subgroup tree. These pathways have featured in several of our studies of mechanisms and symmetry breaking in icosahedral structures and packings [13, 18].

As this section has shown, arrangement of faces and holes on just three polyhedral frameworks has already yielded systems with many, one and no symmetry-detectable mechanisms, respectively. A more general model will encompass all three types of behaviour and show that infinite families with each type of behaviour can be predicted.

4. A model for perforated structures based on cubic polyhedral parents

4.1. Construction

A construction that includes all the examples discussed so far is based on a general cubic polyhedron (a polyhedron whose skeleton is a cubic polyhedral graph, hence a polyhedron with all vertices of degree three). The graph of the starting n-vertex polyhedron P is decorated by addition of an extra vertex of degree two at the midpoint of each edge of P i.e., by edge subdivision of P. The new graph $\mathcal{S}(P)$ is the skeleton of the contact polyhedron C for a perforated structure H with an obvious embedding based on the embedding of P. Figure 3 shows the contact graph common to the examples of W, R and B discussed earlier; in these simple cases, the polyhedron P is the cube.

If P has n vertices, C has n degree-three and $3n/2$ degree-two vertices, representing $5n/2$ bodies, and $3n$ edges representing joints. Each *face* of P corresponds to a *hole* in H. In the most symmetrical realisation, the bodies corresponding to vertices of P would be triangles and those corresponding to edge-midpoints of P would be rectangles (see Figure 4).

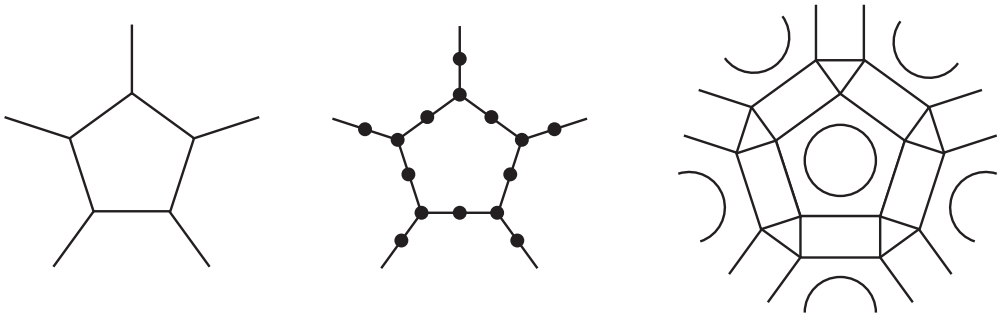

Figure 4: A construction of flexible polyhedra that generalises examples W, R and B. A cubic polyhedron P (left) is subdivided to give the subdivision $\mathcal{S}(P)$ (centre) as the contact graph C of the structure (right) composed of triangular and rectangular rigid plates with holes replacing the original faces of P (indicated by circles).

4.2. Mobility formula

The general expression (3) for the mobility of the object H with contact polyhedron C applies here, but it can also be reformulated in terms of the

parent polyhedron P. As all vertices of C are either original vertices of P, or lie at edge centres of P (Figure 5, top line),

$$\Gamma(v, C) = \Gamma(v, P) + \Gamma(e, P). \tag{12}$$

The edges of C can be taken in symmetric and antisymmetric combinations aligned with the original edges of P, so (Figure 5, bottom line)

$$\Gamma(e, C) = \Gamma(e, P) + \Gamma_{\|}(e, P), \tag{13}$$

where $\Gamma_{\|}(e, P)$ is the representation of a set of vectors along the edges of P. Likewise, the vector representation $\Gamma_{\|}(e, C)$ is equal to the same sum,

$$\Gamma_{\|}(e, C) = \Gamma(e, P) + \Gamma_{\|}(e, P), \tag{14}$$

as no symmetry operation of P has the effect of reversing in place an arrow on one of the derived edges in C.

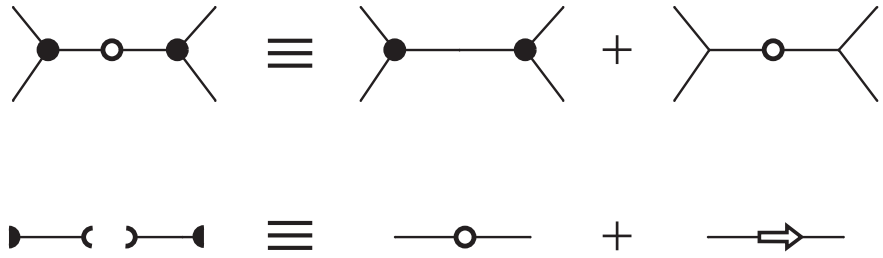

Figure 5: Relations between component symmetries in the contact graph C and its cubic parent P: vertices (top); edges of C (bottom). Vertices common to both P and C are shown as solid circles, vertices that belong to C alone are shown as open circles.

Substitution of (13) and(14) into (3) gives

$$\Gamma(m)-\Gamma(s) = (\Gamma(v, P)-\Gamma_{\|}(e, P)-\Gamma_0)\times(\Gamma_T+\Gamma_R)+\Gamma(e, P)+\Gamma_{\|}(e, P), \tag{15}$$

which could be interpreted as the mobility of an object that has P rather than $\mathcal{S}(P)$ as its contact polyhedron, but has an extra set of mechanisms consisting of 'slides' along the edges of P.

We can go further by taking explicit account of the fact that P is a cubic polyhedron. For a cubic polyhedron, the representation $\Gamma(v, P) \times \Gamma_T$, which

is the symmetry of orthoschemes of local vectors attached to the vertices of P (i.e., the so-called mechanical representation of vibrational theory [33]) is related to edge representations as

$$\Gamma(v,P) \times \Gamma_T = \Gamma(e,P) + \Gamma_\parallel(e,P), \tag{16}$$

implying

$$\Gamma(v,P) \times \Gamma_R = \Gamma(e,P) \times \Gamma_\epsilon + \Gamma_\perp(e,P). \tag{17}$$

Equation (16) is the basis of a force-field model for the vibrations of cubic polyhedral frameworks [3]. For such polyhedra, the freedoms of the vertices, which encompass internal vibrations and rigid-body motions, span the same symmetry as the complete set of edge stretches and edge slides, in contrast to the vibrations of the dual deltahedral frameworks, which can be described by a purely edge-stretching force field.

The edge terms in (15) can be simplified by using spherical-shell theorems for the π representation [26, 27, 16] associated with the edges, i.e., the symmetry of the set of tangential vectors along and across edges:

$$\begin{aligned} \Gamma(e,P) \times \Gamma_T &= \Gamma(e,P) + \Gamma_\parallel(e,P) + \Gamma_\perp(e,P), & (18)\\ \Gamma(e,P) \times \Gamma_R &= \Gamma(e,P) \times \Gamma_\epsilon + \Gamma_\perp(e,P) + \Gamma_\parallel(e,P), & (19) \end{aligned}$$

and hence the terms needed for simplification of (15) are

$$\Gamma_\parallel(e,P) = \Gamma(v,P) \times \Gamma_T - \Gamma(e,P) \tag{20}$$

and

$$\begin{aligned} \Gamma_\parallel(e,P) \times (\Gamma_T + \Gamma_R) &= (\Gamma_\parallel(e,P) + \Gamma_\perp(e,P)) \times \Gamma_T \\ &= (\Gamma(e,P) \times \Gamma_T - \Gamma(e,P)) \times \Gamma_T \\ &= \Gamma(e,P) \times \Gamma_T \times \Gamma_T - \Gamma(e,P) \times \Gamma_T. \end{aligned} \tag{21}$$

Collecting terms, (15) becomes

$$\Gamma(m) - \Gamma(s) = \Gamma(v,P) \times \Gamma_T - \Gamma(e,P) \times \Gamma_\square - (\Gamma_T + \Gamma_R), \tag{22}$$

or,

$$\Gamma(m) - \Gamma(s) + \Gamma_T + \Gamma_R = \Gamma(v,P) \times \Gamma_T - \Gamma(e,P) \times \Gamma_\square, \tag{23}$$

where edge-vector representations have been eliminated at the cost of introducing a new constant representation $\Gamma_\square$ that depends on the group but not on the particular polyhedron and is defined by,

$$\Gamma_\square = \Gamma_T \times \Gamma_T - 2\Gamma_T - \Gamma_\epsilon = (\Gamma_T - \Gamma_0) \times (\Gamma_T - \Gamma_0) - (\Gamma_\epsilon + \Gamma_0). \tag{24}$$

4.3. Character computation

The advantage of the formulation set out in the preceding section is that it reduces the calculation of mobility of the structure H with contact polyhedron C to counting of the edge and vertex elements of P that are in special positions. Specifically, the vertices of a cubic polyhedron can lie on, at most, E, C_3 and σ symmetry elements, and edges can be preserved by at most E, C_2 and σ. Now, Γ_T has trace $\chi_T(C_\phi) = 2\cos\phi + 1$, and hence $\chi_T(C_3) = 0$, and for any reflection $\Gamma_\square$ has trace $\chi_T(\sigma) = 0$. Furthermore, as P is cubic, the trace under the identity is

$$\chi_{\mathrm{RHS}}(E) = m - s + 6 = 3n - 2(3n/2) = 0, \tag{25}$$

which simply re-expresses the net overbracing by six states of self-stress. The only terms on the RHS of (23) that survive under other operations give traces

$$\chi_{\mathrm{RHS}}(C_2) = -2e_2 \tag{26}$$

and

$$\chi_{\mathrm{RHS}}(\sigma) = v_\sigma, \tag{27}$$

where e_2 is the number of edges of P fixed by the given C_2 axis ($e_2 = 2, 1,$ or 0) and v_σ is the number of vertices of P fixed by the given mirror plane.

The mobility of all perforated structures constructed according to the recipe of subdivision of a cubic polyhedral parent can therefore be calculated using a tabular calculation based on (23), but concentrating on C_2 and σ operations only, notionally filling out the reducible character with a zero under all other operations, and then subtracting $\Gamma_T + \Gamma_R$, the representation of the rigid-body motions. Hence for W, the calculation in $\mathcal{O}_h$ needs only the reduced set of columns

Reduced $\mathcal{O}_h$	$6C_2$	$3\sigma_h$	$6\sigma_d$
$\Gamma(v,P)\times\Gamma_T$	0	0	4
$-\Gamma(e,P)\times\Gamma_\square$	-4	0	0
$\Gamma(m)-\Gamma(s)+\Gamma_T+\Gamma_R$	-4	0	4

(with zero $\chi_{\mathrm{RHS}}(R)$ implied for all other operations R) which reduces to $-A_{1u} + A_{2u} + T_{1u} - T_{1u}$, and after subtraction of $\Gamma_T + \Gamma_R = T_{1u} + T_{1g}$, gives

$$\Gamma(m) - \Gamma(s) = A_{2u} - A_{1u} - T_{1g} - T_{2u},$$

exactly as calculated from (23) with the full character table.

The vertex/edge form (23) for the mobility criterion is well adapted to treatments of infinite families of structures built from cubic polyhedra and results are listed in the next section. These include calculation of the mobility of structures derived from subdivision of polyhedra belonging to the families of prisms (and their relatives, the wedges and barrels), multilayer prisms, leapfrogs and quadruples, as shown in the following.

5. Examples

5.1. Prisms as parents P

The $[N]$-prism has two faces of size N, and N faces of size 4. It is convenient to treat odd and even prisms separately.

The odd prism has two distinguished faces of size $N = (2p + 1)$, with maximum point-group symmetry $\mathcal{D}_{(2p+1)h}$, which is a subgroup of the group of the centro-symmetric cylinder, $\mathcal{D}_{\infty h}$. Calculations can be carried out in the higher group retaining only C_2', σ_v and σ_h symmetry elements. Reflection in the horizontal mirror plane shifts all vertices. An odd prism has $v_\sigma = 2$ for the $(2p + 1)$ σ_v reflections, and $e_2 = 1$ for the $(2p + 1)$ C_2' rotations.

The mobility representation for a system with contact graph C formed by the subdivision is therefore

$$\mathcal{D}_{\infty h}: \qquad \Gamma(m) - \Gamma(s) = -\Sigma_u^+ - \Sigma_u^- - \Pi_u - \Pi_g, \tag{28}$$

or, for finite p,

$$\mathcal{D}_{(2p+1)h}: \qquad \Gamma(m) - \Gamma(s) = -A_1'' - A_2' - E_1' - E_1''. \tag{29}$$

Symmetry has therefore detected six states of self-stress but no mechanism for systems based on the odd prism.

On the other hand, the even prism has two distinguished faces of size $N = 2p$, with maximum point-group symmetry $\mathcal{D}_{2ph}$ (or exceptionally, for $p = 2$, $\mathcal{O}_h$). The even prisms do not extrapolate to the $\mathcal{D}_{\infty h}$ supergroup, as for all finite p there are two classes of vertical mirror planes and two classes of C_2 axes perpendicular to the main axis. However, extrapolation along the series $\mathcal{D}_{4h}, \mathcal{D}_{6h}, \mathcal{D}_{8h}, \mathcal{D}_{10h}$ [1] shows the appropriate limiting form of the representations. An even prism has $v_\sigma = 4$ for σ_d, and $v_\sigma = 0$ for σ_v, $e_2 = 0$ for C_2', and $e_2 = 2$ for C_2'' operations and for the C_2 operation associated with the principal axis. Calculations must be carried out separately for $N = 4q+2$ and $N = 4q$. The mobility representation for a system with contact graph C formed by the subdivision of the even prism is

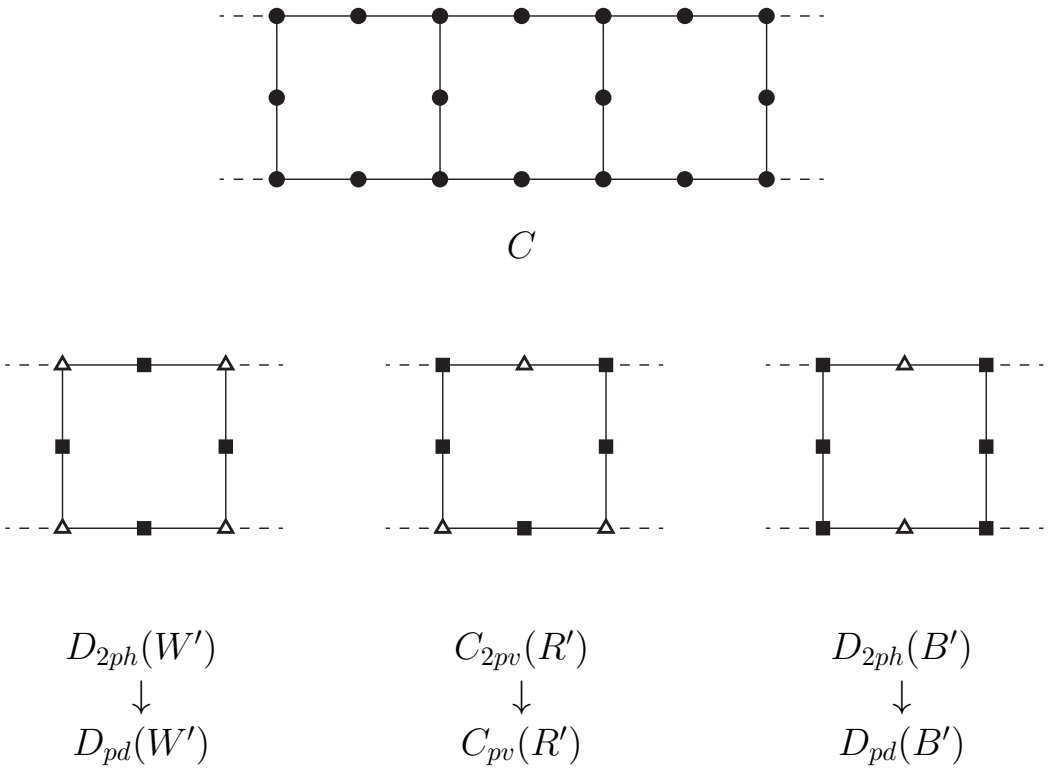

Figure 6: Non-isomorphic flexible perforated polyhedra based on a single contact graph. C is the contact graph formed by subdivision of the $[2p]$-prism. W′, R′ and B′ are symmetrical realisations with $4p$ triangular and $6p$ rectangular bodies. All three have single mechanisms giving initial descent to a halving point group, as indicated. For $2p = 4$, W′ can achieve the higher $\mathcal{O}_h$ symmetry, with initial descent to $\mathcal{T}_d$.

$\mathcal{D}_{(4q+2)h}$: $\Gamma(m) - \Gamma(s) = B_{1g} - A_{1u} - A_{2g} - B_{2g} - E_{1g} - E_{1u}$; (30)

$\mathcal{D}_{(4q)h}$: $\Gamma(m) - \Gamma(s) = B_{1u} - A_{1u} - A_{2g} - B_{2u} - E_{1g} - E_{1u}$. (31)

Symmetry detects seven states of self-stress and a non-degenerate mechanism for all even-prism parents. The B_{1g}/B_{1u} symmetry of the mechanism implies a motion where alternate three-coordinate vertices of C move up and down parallel to the main axis, with top and bottom rings moving in phase.

5.2. Wedges as parents P

Further results for two families related to prisms are straightforwardly obtained. The first is the family of *wedges*. From any $[N+1]$-prism it is possible to construct a cubic polyhedron with $n = 2N$ vertices that has two faces of the maximum possible size, which is $N + 1$. This is done by 'squeezing out' one square face from between top and bottom faces of the prism. More precisely, the $[N]$-wedge polyhedron has two faces of size N that share a common edge, which also links two triangular faces; the remaining $N - 3$ faces are square. For $N > 3$, the point group symmetry of the wedge polyhedron is $\mathcal{C}_{2v}$. Subdivision of the edges leads to the contact graph of a perforated polyhedron which has no symmetry-detected mechanism, but six states of self-stress that span representations $-A_1 - 3A_2 - B_1 - B_2$ (odd N), or $-A_1 - 2A_2 - B_1 - 2B_2$ (even N) in $\mathcal{C}_{2v}$. Hence, the symmetry approach predicts all wedges to be rigid.

5.3. Barrels as parents P

The second family derived from prisms comprises the *barrels*. The $[N]$-barrel is constructed by placing two N-gons as in a prism and replacing the central cyclic strip of square faces by a cycle of $2N$ vertices joined alternately to vertices in top and bottom faces. The resulting polyhedron has $2N$ pentagonal faces, N in the corona of each N-gonal face. An example is shown as a Schlegel diagram in Figure 5.3. The symmetry of the $[N]$-barrel is $\mathcal{D}_{Nd}$, the point group of the $[N]$-antiprism; for the special case of $N = 5$, there is the possibility of achieving $\mathcal{I}_h$ symmetry when the [5]-barrel is equilateral and coincides with the regular dodecahedron.

The symmetry treatment of perforated polyhedra with D_{Nd} barrels as parents predicts in every case a single mechanism, in spite of the obvious overbracing of the construction. Each barrel has no edges on the principal axis, two edges on each C_2' axis, and four vertices in each σ_d plane, and hence

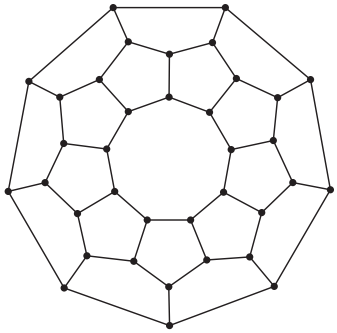

Figure 7: Schlegel diagram of the $[N]$-barrel with $N = 9$.

by (26) and (27) has mobility representation $B_2 - A_2 - 2B_1 - E_1 - E_{N-1}$ for even N, and $A_{2u} - 2A_{1u} - A_{2g} - E_{1g} - E_{1u}$ for odd N. The mechanism has the symmetry of a translation along the principal axis.

Case of $N = 5$ in maximum $\mathcal{I}_h$ symmetry, is special. In the $\mathcal{I}_h$ group, the symmetry approach detects a triply degenerate mechanism and nine states of self-stress (see equation (11)). Descent in symmetry from $\mathcal{I}_h$ to $\mathcal{D}_{5d}$, a choice consistent with restriction of equivalence to the $2N$ pentagonal faces around the body of the barrel, gives $T_{2u} \to A_{2u}+E_{2u}$, $T_{1g} \to A_{2g}+E_{1g}$, $A_u \to A_{1u}$ and $H_u \to A_{1u}+E_{1u}+E_{2u}$, and the triply degenerate mechanism breaks up into a single mechanism of A_{2u} symmetry and a pair of E_{2u} symmetry. In the lower symmetry group, the pair is equisymmetric with a pair of states of self-stress and hence no longer gives rise to a mechanism that is detectable by symmetry. The surviving A_{2u} mechanism has the symmetry of a translation along the principal axis, even though the T_{2u} set of mechanisms in $\mathcal{I}_h$ corresponds to a set of cubic harmonics, rather than to the cartesian triple $\{x, y, z\}$.

5.4. Families of non-isomorphic perforated polyhedra based on a common contact graph

The objects W, R and B are examples of this type. All have the same contact polyhedron (the subdivision of the cube), and essentially differ only in the point-group symmetry imposed by the specifics of the various bodies and hence the embedding of that contact graph in space. As noted in the introduction, the three objects are related by rotations of layers of bodies with respect to a C_4 axis. A straightforward extension is to apply this rotation

technique to the realisations of the contact polyhedron that arises from subdivision of the $[2p]$-prism. (See Figure 6.) If the bodies are arranged in three layers (top: an alternating cycle of $2p$ triangles and $2p$ rectangles; middle: an alternating cycle of $2p$ squares and $2p$ holes; bottom: as top layer), we can construct analogues W′, R′ and B′ of W, R and B.

It is easy to see that all three cases have the same representation $\Gamma(m) - \Gamma(s)$ as that calculated for the subdivision of the even prism (Section 5.1) in the appropriate point group, and that all will share the same symmetry-detected mechanism.

5.5. Inflated cubic polyhedra as parents P

Cubic polyhedra can be inflated to yield other cubic polyhedra using the family of Goldberg-Coxeter transformations [8, 14]. Two transformations of interest in applications to fullerenes for example are the leapfrog $\mathcal{L}$ and quadrupling $\mathcal{Q}$ inflations [17]. Both preserve the point group symmetry of the parent. Given an n-vertex parent P, $\mathcal{L}$ produces a cubic polyhedron with $3n$ vertices, and $\mathcal{Q}$ produces one with $4n$ vertices.

The various reducible representations for sets of structural components of the polyhedra $\mathcal{L}(P)$ and $\mathcal{Q}(P)$ can be derived from those of P. These relations suggest some interesting questions about the effects of transformations on perforated polyhedra.

5.5.1. Leapfrog polyhedra as parents

The leapfrog operation can be described in several equivalent ways, one of which is illustrated in Figure 8. Each face of P is replaced by a rotated inset of itself, and all new vertices are joined by edges perpendicular to the original edges of P; vertices and edges of P are then discarded.

For leapfrogs of cubic polyhedra [17],

$$\Gamma(v, \mathcal{L}(P)) = \Gamma(v, P) \times \Gamma_R + \Gamma(e, P) - \Gamma(e, P) \times \Gamma_\epsilon \tag{32}$$

and

$$\Gamma(e, \mathcal{L}(P)) = \Gamma(v, P) \times \Gamma_T + \Gamma(e, P). \tag{33}$$

Consider two perforated polyhedra. One is derived from P, i.e., it has contact graph $C = \mathcal{S}(P)$. The other is derived from $\mathcal{L}(P)$ and has contact graph $\mathcal{S}(\mathcal{L}(P))$. Mobilities of each can be calculated in $\mathcal{G}$, the point group of both P and $\mathcal{L}(P)$, using (23). We can ask the question: When is the

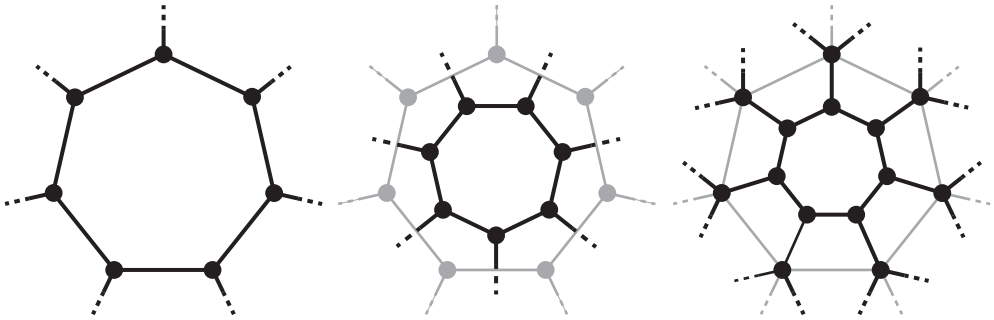

Figure 8: Transformation of faces of polyhedon P under leapfrog ($\mathcal{L}(P)$) and quadrupling ($\mathcal{Q}(P)$) transformations.

symmetry-predicted mobility $\Gamma(m)-\Gamma(s)$ equal for the perforated polyhedra based on a polyhedron P and its leapfrog?

Define the mobility difference Γ_{LP} as the representation $\Gamma(m)-\Gamma(s)$ calculated with parent $\mathcal{L}(P)$ minus $\Gamma(m)-\Gamma(s)$ calculated with P as parent. This representation is

$$\Gamma_{LP} = \Gamma(v,P)\times\{\Gamma_R-\Gamma_0-\Gamma_\square\}\times\Gamma_T - \Gamma(e,P)\times\{\Gamma_R-\Gamma_T\}. \qquad (34)$$

Γ_{LP} has character zero under all but reflection operations, for which $\chi_{LP}(\sigma) = 2e_\parallel + 2e_\perp - 2v_\sigma = 2(e_\perp - e_\parallel)$, where $e_\parallel$ and $e_\perp$ are respectively the numbers of edges of P lying in and crossing the σ mirror plane, and v_σ is the number of vertices of P lying in that plane. The same result for $\chi_{LP}(\sigma)$ could be derived by noting that leapfrogging affects $e_\parallel$ and $e_\perp$ as follows: $e_\parallel(\mathcal{L}(P)) = e_\perp(P) = \frac{1}{2}v_\sigma(\mathcal{L}(P))$ and $e_\perp(\mathcal{L}(P)) = 3e_\parallel(P)$.

By either route, various conditions applying to equality of $\Gamma(m)-\Gamma(s)$ for perforated polyhedra with $C=\mathcal{S}(\mathcal{L}(P))$ and $C=\mathcal{S}(P)$ can be derived. The two structures have the *same* $\Gamma(m)-\Gamma(s)$ if P is chiral, i.e., belongs to a pure rotational group $\mathcal{C}_n$, $\mathcal{D}_n$, $\mathcal{T}$, $\mathcal{O}$, $\mathcal{I}$, or P is achiral but belongs to a group that contains no reflection elements, i.e., $\mathcal{C}_i$, $\mathcal{S}_{2n}$.

The smallest chiral cubic polyhedron has $n=10$ vertices (see e.g., [15]) and is of $\mathcal{C}_2$ symmetry. All perforated polyhedra with $\mathcal{C}_2$ parents are without symmetry-detectable mechanisms as $\Gamma(m)-\Gamma(s)$ has $\chi(E)=-6$ and $\chi(C_2)=2=-e_2$, and so is $-(2+e_2)A-(1+e_2)B$. Similar reasoning shows that all perforated polyhedra with $\mathcal{D}_2$ or $\mathcal{D}_N$ (N odd) parents also

lack symmetry-detectable mechanisms. Symmetry-detectable mechanisms are, however, possible for $\mathcal{D}_4$ and $\mathcal{D}_6$ parents P.

The two structures have *different* $\Gamma(m)-\Gamma(s)$ if P is bipartite and belongs to a group with a reflection plane, i.e., $\mathcal{C}_s$, $\mathcal{C}_{nh}$, $\mathcal{C}_{nv}$, $\mathcal{D}_{nh}$, $\mathcal{D}_{nd}$, $\mathcal{T}_d$, $\mathcal{T}_h$, $\mathcal{O}_h$, $\mathcal{I}_h$; this follows as a bipartite polyhedron has only even faces, and any mirror plane cuts the polyhedron with either $e_\parallel \neq 0$ and $e_\perp = 0$ or $e_\parallel = 0$ and $e_\perp \neq 0$.

When P is non-bipartite and belongs to a group with one or more mirror planes, the two perforated polyhedra share mobility $\Gamma(m)-\Gamma(s)$ if $e_\parallel = e_\perp$ for every mirror plane. Examples include those with P the tetrahedron (leapfrog = truncated tetrahedron) and the dodecahedron (leapfrog = truncated icosahedron, skeleton of the C_{60} molecule).

Double leapfrogging restores the orientation of those faces derived from the original parent. From (32), (33)and (34) it follows that if structures with $C = \mathcal{S}(P)$, $C = \mathcal{S}(\mathcal{L}P)$, and $C = \mathcal{S}(\mathcal{L}^2P)$ are all to share a common mobility $\Gamma(m) - \Gamma(s)$, it is necessary to have $e_\parallel(P) = e_\perp(P) = v_\sigma(P) = 0$ for every reflection plane σ. This condition can be achieved if and only if parent P has no reflection planes. In particular, all chiral parents P give an infinite chain of perforated polyhedra based on $C = \mathcal{S}(\mathcal{L}^q(P))$, $q = 0, 1, \ldots$ that all share the same mobility.

5.5.2. Quadrupled cubic polyhedra as parents

In quadrupling, each face of P is replaced by an unrotated inset of itself and new vertices are joined by new edges to the corresponding original vertices of P; all original edges of P are discarded (see Figure 8).

For quadruples of cubic polyhedra,

$$\Gamma(v, \mathcal{Q}(P)) = \Gamma(v, P) + \Gamma(v, P) \times \Gamma_T \tag{35}$$

and

$$\begin{aligned} \Gamma(e, \mathcal{Q}(P)) &= \Gamma(v, P) \times \Gamma_T + \Gamma(e, P) + \Gamma_\perp(e, P) \\ &= \Gamma(v, P) \times (\Gamma_T + \Gamma_R) + \Gamma(e, P) \times (\Gamma_0 - \Gamma_\epsilon), \end{aligned} \tag{36}$$

and hence from (23), the mobility of a structure whose parent is $\mathcal{Q}(P)$, i.e., of a structure with contact graph $C = \mathcal{S}(\mathcal{Q}(P))$, can be written in terms of the vertex and edge representations of the original polyhedron P as

$$\begin{aligned} \Gamma(m) - \Gamma(s) + \Gamma_T + \Gamma_R &= \Gamma(v, P) \times \{\Gamma_0 + \Gamma_T - \Gamma_\square - \Gamma_\epsilon \times \Gamma_\square\} \times \Gamma_T \\ &\quad -\Gamma(e, P) \times \{\Gamma_0 - \Gamma_\epsilon\} \times \Gamma_\square\}. \end{aligned} \tag{37}$$

In this equation, the RHS has non-zero trace only for reflection planes σ, where $\chi(\sigma)$ is $4e_{\|}(P)$. A simple consequence is that $\Gamma(m) - \Gamma(s)$ for $C = \mathcal{S}(\mathcal{Q}(P))$ includes *no* mechanism detectable by symmetry if P belongs to a point group without mirror planes.

Quadrupling can preserve the mobility $\Gamma(m) - \Gamma(s)$ in other circumstances. Perforated polyhedra with $C = \mathcal{S}(P)$ and $C = \mathcal{S}(\mathcal{Q}(P))$ can share the same mobility, e.g., when $v_\sigma = 2e_{\|} = 0$, as in a cylindrical polyhedron of appropriate symmetry that has a belt of zig-zag hexagonal faces.

6. Connection with the Hobermann Switch-Pitch

The Hobermann Switch-Pitch is a toy that presents a tetrahedrally symmetric (T) exterior, and exhibits a transformation from a symmetric covering of the sphere that switches between two visually different closed forms when tossed in the air. This inside-out transformation is accomplished by movement along a unique mechanism, as the structure passes through a high-symmetry open configuration of O symmetry. The manufactured object has special gearing to restrict the motion to a single mechanism that passes through any potential multifurcation points with preservation of symmetry. The lack of reflection symmetry at all points along the pathway is not intrinsic to the nature of the mechanism, but is caused by an aesthetic choice of the shapes for the moving parts. These superficial differences disappear at the level of the contact graph, C. As a graph, C is identical with that derived from W, and, if we move up to the O_h supergroup and down to O, the symmetry analysis [4] proceeds exactly as in section 3, with deletion of all improper operations in the case of the Switch-Pitch. Thus, $\Gamma(m) - \Gamma(s)$ is exactly as in (4) after removal of g/u labels, and hence predicts a mechanism that entails descent in symmetry from O to T.

We note that this connection between the Switch-Pitch and the perforated polyhedron W has also been observed by Walter Whiteley and communicated to the present authors.

7. Conclusion

Symmetry extension of counting rules has been shown to explain observations of mobility in some heavily overconstrained systems and to suggest several classes of generalised objects where flexibility also survives the overbracing. Necessary conditions for such mobility take the form of counts

applied under key elements of symmetry, and typically improve on the standard mobility count, which can be seen as counting under the identity element alone.

Acknowledgements

We thank Walter Whiteley, Bob Connelly and Barbara Heys for helpful discussions.

References

[1] Altmann, S. L. and Herzig, P. (1994). *Point-Group Theory Tables*. Clarendon Press, Oxford.

[2] Atkins, P. W., Child, M. S., and Phillips, C. S. G. (1970). *Tables for Group Theory*. Oxford University Press.

[3] Ceulemans, A., Titeca, B. C., Chibotaru, L. F., Vos, I., and Fowler, P. (2001). Complete bond force fields for trivalent and deltahedral cages: group theory and applications to cubane, closo-dodecaborane and buckminsterfullerene. *Journal of Physical Chemistry A*, 105:8284–8295.

[4] Chen, Y., Guest, S. D., Fowler, P. W., Feng, J., Wei, G., and Dai, J. (2015). Mobility and symmetry analysis of the Hoberman Switch-Pitch structure and a class of polyhedral generalisations. In preparation.

[5] Connelly, R., Fowler, P. W., Guest, S. D., Schulze, B., and Whiteley, W. (2009). When is a pin-jointed framework isostatic? *International Journal of Solids and Structures*, 46:762–773.

[6] Cruickshank, J., Kitson, D., and Power, S. (2015). The generic rigidity of triangulated spheres with blocks and holes. *preprint, arXiv:1507.02499*.

[7] Cundy, H. M. and Rollett, A. P. (1961). *Mathematical Models*. Oxford University Press.

[8] Dutour, M. and Deza, M. (2004). Goldberg-Coxeter construction for 3- and 4-valent plane graphs. *The Electronic Journal of Combinatorics*, 11:R20.

[9] Finbow-Singh, W., Ross, E., and Whiteley, W. (2012). The rigidity of spherical frameworks: Swapping blocks and holes in spherical frameworks. *SIAM J. Discrete Math.*, 26(1):280–304.

[10] Finbow-Singh, W. and Whiteley, W. (2013). Isostatic block and hole frameworks. *SIAM J. Discrete Math.*, 27(2):991–1020.

[11] Fowler, P. W. and Guest, S. D. (2000). A symmetry extension of Maxwell's rule for rigidity of frames. *International Journal of Solids and Structures*, 37:1793–1804.

[12] Fowler, P. W. and Guest, S. D. (2002). Symmetry and states of self stress in triangulated toroidal frames. *International Journal of Solids and Structures*, 39(17):4385–4393.

[13] Fowler, P. W., Guest, S. D., and Tarnai, T. (2008). A symmetry treatment of danzerian rigidity for circle packing. *Proceedings of the Royal Society: Mathematical, Physical and Engineering Sciences*, 464:3237–3254.

[14] Fowler, P. W. and Manolopoulos, D. E. (2006). *An Atlas of Fullerenes*. Dover Publications.

[15] Fowler, P. W. and Mitchell, D. (1996). A sum rule for symmetries and isomer counts of trivalent polyhedra. *Journal of the Chemical Society Faraday Transactions*, 92:4145–4150.

[16] Fowler, P. W. and Quinn, C. M. (1986). σ, π and δ representations of the molecular point groups. *Theoretica Chimica Acta*, 70:333–350.

[17] Fowler, P. W. and Redmond, D. B. (1992). Symmetry aspects of bonding in carbon clusters: the leapfrog transformation. *Theoretica Chimica Acta*, 83:367–375.

[18] Guest, S. D. (1999). Mechanisms of the icosahedral compound of ten tetrahedra. *Periodica Mathematica Hungarica*, 39:213–223.

[19] Guest, S. D. and Fowler, P. W. (2005). A symmetry-extended mobility rule. *Mechanism and Machine Theory*, 40:1002–1014.

[20] Guest, S. D. and Fowler, P. W. (2007). Symmetry conditions and finite mechanisms. *Journal of Mechanics of Materials and Structures*, 2(2):293–301.

[21] Guest, S. D. and Fowler, P. W. (2010). Mobility of 'N-loops'; bodies cyclically connected by intersecting revolute hinges. *Proceedings of the Royal Society A: Mathematical, Physical and Engineering Science*, 466:63–77.

[22] Guest, S. D., Schulze, B., and Whiteley, W. (2010). When is a symmetric body-bar structure isostatic? *International Journal of Solids and Structures*, 47:2745–2754.

[23] Hoberman, C. (2004). Geared expanding structures. U.S. Patent No. US007464503B2.

[24] Hunt, K. H. (1978). *Kinematic Geometry of Mechanisms*. Clarendon Press, Oxford.

[25] Kangwai, R. D. and Guest, S. D. (1999). Detection of finite mechanisms in symmetric structures. *International Journal of Solids and Structures*, 36(36):5507–5527.

[26] Quinn, C. M., McKiernan, J. G., and Redmond, D. B. (1983). Mollweide projections: molecular-orbital symmetries on the spherical shell, tetrahedral and other symmetries, and δ-orbitals in metal clusters. *Inorganic Chemistry*, 22:2310–2315.

[27] Quinn, C. M., McKiernan, J. G., and Redmond, D. B. (1984). The spherical-shell technique for molecular wavefunctions: some new theorems in group theory. *Journal of Chemical Education*, 61:569–572.

[28] Röschel, O. (2012). A fulleroid-like mechanism based on the cube. *Journal for geometry and graphics*, 16:19–27.

[29] Rouse Ball, W. W. and Coxeter, H. S. M. (1987). *Mathematical Recreations and Essays, 13th Edition*. Dover, New York.

[30] Schulze, B. (2010). Symmetry as a sufficient condition for a finite flex. *SIAM Journal on Discrete Mathematics*, 24(4):1291–1312.

[31] Schulze, B., Guest, S. D., and Fowler, P. W. (2014). When is a symmetric body-hinge structure isostatic? *International Journal of Solids and Structures*, 51:2157–2166.

[32] Schulze, B. and Whiteley, W. (2011). The orbit rigidity matrix of a symmetric framework. *Discrete & Computational Geometry*, 46(3):561–598.

[33] Wilson, E. B., Decius, J. C., and Cross, P. C. (1955). *Molecular Vibrations*. Dover N.Y.